Langmuir

Article

pubs.acs.org/Langmuir

Porous Aromatic Frameworks Impregnated with Fullerenes for Enhanced Methanol/Water Separation

Afsana Ahmed,[‡,†] Zongli Xie,[†] Kristina Konstas,[†] Ravichandar Babarao,[†] B. D. Todd,[‡] Matthew R. Hill,[†] and Aaron W. Thornton*[,†]

[‡]Department of Mathematics, School of Science, Faculty of Science, Engineering and Technology and Centre for Molecular Simulation, Swinburne University of Technology, Melbourne, Victoria 3122, Australia

[†]CSIRO Manufacturing Flagship, Private Bag 33, Clayton South MDC, Victoria 3169, Australia

Supporting Information

ABSTRACT: Molecular simulation techniques have revealed that the incorporation of fullerenes within porous aromatic frameworks (PAFs) remarkably enhances methanol uptake while inhibiting water uptake. The highest selectivity of methanol over water is found to be 1540 at low pressure (1 kPa) and decreases gradually with increasing pressure. The adsorption of water is very small compared to methanol, a useful material property for membrane and adsorbent-based separations. Grand canonical Monte Carlo (GCMC) simulations are utilized to calculate the pure component and mixture adsorption isotherms. The water and methanol mixture simulations show that water uptake is further inhibited above the pure component results because of the dominant methanol adsorption. Molecular dynamics (MD) simulations confirm that water diffusivity is also inhibited by strong methanol adsorption in the mixture. Overall, this study reveals profound hydrophobicity in C_{60}@PAF materials and recommends C_{60}@PAFs as suitable applicants for adsorbent and membrane-based separations of methanol/water mixtures and other alcohol/water separation applications.

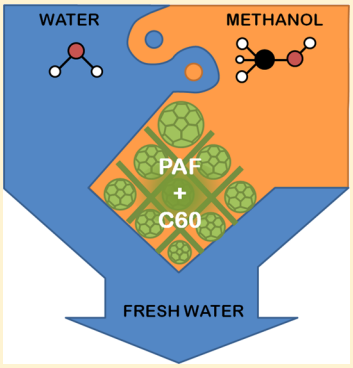

1. INTRODUCTION

The separation of methanol/water (CH_3OH/H_2O) mixtures is an important process in many industrial applications. Conversion of methanol to gasoline produces a large amount of water as a reaction byproduct which must be removed.[1] For large-scale methanol production from natural gas, water is also a byproduct from which methanol recovery systems are required.[1] In general, distillation can be used to remove these organic compounds from water. But if the organic concentrations are very low or the organic compounds are thermally sensitive, then distillation is not economically suitable.[2] Alternative technologies such as adsorbent- and membrane-based separations can be more energy efficient than traditional distillation techniques.[3]

Pervaporation is a membrane separation process which is simple and avoids the problems associated with traditional technologies. It can remove organic solvents from aqueous solutions by the selective transport of the organic phase.[4] Selective transport relies on the difference in diffusivity and solubility (or adsorption uptake) of the organic and aqueous components within the pore network of the membrane material.[3] Another material-based separation technology is the adsorbent-based system, whereby large columns are filled with materials such as zeolites or activated carbons which capture a component of the mixture as it flows through.[5] A desorption stage is then followed with a pressure or temperature swing. Both separation techniques require material characteristics that are favorable for the adsorption and diffusion of one component over its counterpart.[6]

Because of their high surface areas, tunable pore sizes, and stability under pressure-swing and temperature-swing conditions, porous aromatic frameworks (PAFs) have attracted considerable interest in the past 5 years for the adsorption and separation of gases.[7−11] PAFs are organic networks composed of connected phenyl-based ligands forming diamond-like morphologies at the nanoscale range. They possess intrinsically high surface areas and internal volumes, and these factors are known to enhance gas storage.[12] Most of the experimental and theoretical studies for the applications of PAFs were focused on gas storage and separation in recent years.[8,13−25] Adsorption of various gases in PAFs was simulated and compared with experimental data to test the validity of proposed atomic models.[13,19] In addition to high gas storage capacities and separation factors, it has recently been shown that PAFs interact strongly within porous polymers providing stability against the well-known aging effects that highly porous polymers suffer from in membranes.[26]

Membranes are generally diffusion-based while adsorbents are adsorption-controlled. Zheng and co-workers[27] found from their molecular dynamics simulations that the transport of a mixture of water and methanol through hydrophobic tubes is faster than through hydrophilic nanotubes due to a hydrogen network. Palinkas et al.[28] had used a flexible three-site methanol model for

Received: September 9, 2014
Revised: November 5, 2014
Published: November 7, 2014

   dx.doi.org/10.1021/la503547n | Langmuir 2014, 30, 14621−14630

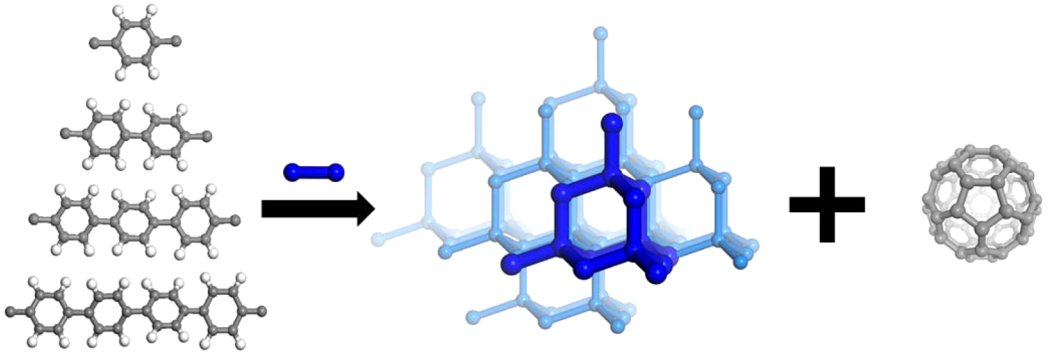

Figure 1. Schematic of porous aromatic frameworks formed with various ligands and then impregnated with fullerenes.

the calculation of self-diffusivity of bulk methanol at 286 K. In addition, there are some recent studies that have investigated the adsorption and diffusion of water and alcohols in metal−organic frameworks (MOFs).[29−32] Chen et al.[33] have investigated adsorption and separation of CH_3OH/H_2O by integrating experiment and simulation for $Zn(BDC)(TED)_{0.5}$, a highly hydrophobic MOF. They have reported that H_2O adsorption is vanishingly small compared to the strong adsorption of CH_3OH. The highest selectivity of CH_3OH over H_2O at 1 kPa is approximately 20 and decreased with increasing pressure. Nalaparaju et al.[29] have performed MD simulation to calculate adsorption of water and alcohols in hydrophilic and hydrophobic zeolitic MOFs (ZMOFs). For hydrophilic Na-rho-ZMOF framework water adsorption increases continuously with increasing pressure and replaces alcohols competitively at high pressures. Again, for hydrophobic ZIF-71, alcohols are selectively adsorbed at low pressures but exceeded by water with increasing pressure.

On the basis of these previous studies, we propose that fullerene-impregnated PAFs are good candidates for the separation of CH_3OH/H_2O mixtures and other alcohol or organic/water-based separations, as illustrated in Figure 1. PAFs and fullerenes are both inherently hydrophobic, and their combination will offer the further tuning of porosity to enhance separations. Because of the hydrophobic nature of the composite and the hydrophobic solvent carbon disulfide, impregnation is feasible, and the volatility of the solvent means it can be easily removed under dynamic vacuum and thermal treatment. This has been experimentally confirmed within our group and will be subject of a future article.

In this paper we aim to understand the adsorption and diffusion behavior of methanol and water mixtures within the composite material using molecular simulation techniques. The simulation technique to examine the adsorption and separation of the CH_3OH/H_2O mixture in fullerene-impregnated PAF-30X (X = 2−4) is investigated in this work. Our main objective is to present a clear understanding of sorption behavior in these PAFs at a molecular level. In the spirit of our previous work,[34] we also aim to provide experimental guidelines for the optimal impregnation amount of fullerenes to maximize separation performance.

2. SIMULATION MODELS AND METHODS

2.1. Adsorption Model. In this work the PAF structures were constructed according to Lan et al.[8] The structures include PAF-30X (X = 1−4), where 3 means 3D structure and X denotes the number of phenyl rings used to replace the C−C bond of a diamond morphology. Each unit cell was constructed using the Forcite module of the Material Studio package with cubic periodic boundaries.[35] Fullerenes (C_{60}) were randomly inserted within the PAF unit cell followed by geometry optimization, forming the nC_{60}@PAF composite. In reality, PAFs are generally amorphous systems with local order, and therefore the crystal model is a good approximation of the system. Interpenetration is likely to occur for long ligands which is likely to exhibit similar adsorption behavior to impregnation, though the pore shapes will be quite different.

The prediction of CH_3OH and H_2O uptake inside the nC_{60}@PAF structures was calculated by the grand canonical Monte Carlo (GCMC) routine. GCMC simulations were carried out for the adsorption of mixtures and single components in the framework with modified Dreiding force field (Table S1 in Supporting Information) within the Material Studio package.[36,37] As a widely used technique to simulate adsorption, GCMC allows us to relate the chemical potentials of adsorbate in both adsorbed and bulk phases. In this method, the sorbate structures (CH_3OH and H_2O) and the sorbent structure (nC_{60}@PAF) are treated as rigid. The rigid model has proved accurate in many MD simulation studies,[38−41] and it is suitable to reproduce the critical parameters and saturated liquid densities of alcohol.[42] Trial addition, deletion, translation, and rotation moves of the CH_3OH and H_2O molecules are repeated and accepted/rejected based on the grand canonical ensemble at specific temperature and pressure. 10^7 trial moves were used for equilibration and another 10^7 moves for production steps for ensuring an accurate average.

For H_2O and CH_3OH adsorption simulation in PAFs and nC_{60}@PAFs, we only considered the electrostatic interactions of the atoms in the H_2O and CH_3OH molecules and ignored the atomic charges of the PAFs and nC60@PAFs which are found to be negligible. Yang et al.[43] have investigated the effect of charge on PAFs for CO_2 storage and separation in PAFs. They compared their results with Babarao et al.'s data considering the atomic charges of the PAFs.[17] Their results were close to the experimental data and Babarao et al.'s results, indicating that charges are negligible. We have also tested the effect of charge for adsorption data of an equimolar mixture of H_2O and CH_3OH and found there is minimal effect (see Figures S1 and S2). Therefore, it is not necessary to consider the atomic charges for the nanoporous materials without metal or heavy atoms.

H_2O was mimicked by the three-point transferable interaction potentials (TIP3P) model.[33] The O−H bond length was 0.9572 Å, and the angle between H and O−H was 104.52°. Previous research shows that the TIP3P model always offers noble interaction potentials compared to experimental values of adsorption.[44−46] TIP3P was used here because of its simplicity,

dx.doi.org/10.1021/la503547n | Langmuir 2014, 30, 14621−14630

accuracy, and computational efficiency. The electrostatic interaction of H_2O and CH_3OH followed Coulomb's law, and the dispersion and repulsion forces were calculated by the Lennard-Jones potential

$$U_{ij}(r) = \sum_{\substack{\alpha\epsilon i \\ \beta\epsilon j}} 4\varepsilon_{\alpha\beta}\left[\left(\frac{\sigma_{\alpha\beta}}{r_{\alpha\beta}}\right)^{12} - \left(\frac{\sigma_{\alpha\beta}}{r_{\alpha\beta}}\right)^{6}\right] + \frac{q_\alpha q_\beta}{4\pi\varepsilon_0 r_{\alpha\beta}}$$

where U_{ij} is the internal energy, $r_{\alpha\beta}$ is the distance between two atoms, $\sigma_{\alpha\beta}$ and $\varepsilon_{\alpha\beta}$ are collision diameter and potential well depth, respectively, and q_α and q_β are partial charges located at site α and β, respectively. The long-range Coloumbic forces were handled by Ewald summation technique for all of our calculations. Lorentz−Berthelot rule mixing rules have been used to calculate the interaction between H_2O and CH_3OH and C_{60}@PAFs.[47] The set of parameters for the CH_3OH model were adopted from the transferable potentials for phase equilibria force field and are summarized in Table 1.[48] This three-site

Table 1. Force Field Parameters for H_2O and CH_3OH[33]

		LJ and Coulombic potential				
species	site	σ (Å)	ε/k_B (K)	q (e)	bond length (Å)	bending angle (deg)
H_2O	O	3.151	76.47	−0.834	r_{H-O} = 0.9527	$\theta_{\angle HOH}$ = 104.52
	H	0	0	+0.417		
CH_3OH	CH_3	3.775	104.17	+0.265	r_{CH_3-O} = 1.4246	
	O	3.071	85.85	−0.700	r_{O-H} = 0.9451	$\theta_{\angle CH_3OH}$ = 108.53
	H	0	0	+0.435		

model has been used to predict a range of properties that are in good agreement with the available experimental values.[39,42,49−51] The classical level of theory is used in this study without the inclusion of quantum or polarization effects. It is unlikely that mirror charges will form from polarization effects because the assigned charges are relatively weak.

2.2. Diffusion Model. Diffusion (or diffusivity) is predicted using a series of molecular dynamics simulations based on Newton's laws of motion. The same modified Dreiding force field has been implemented as described above. For the H_2O model, we have used the same TIP3P model as described above for adsorption. The force field for CH_3OH was tested at bulk phase conditions to compare with experimental bulk diffusivity values. For nonbonded interactions between molecules a spherical cutoff radius of 0.9 nm was used in all cases. The amount of guest molecules and fullerenes within the material was determined from the previous adsorption simulations. In this study the fullerenes are considered fixed during the molecular simulation. Previous studies have suggested that the binding energy of fullerenes within the material is strong enough to hold the fullerenes in place.[52] In the NVT ensemble, the Nosé−Hoover thermostat was used with an average temperature of 303 K at fixed cell volume and number of atoms within a fully periodic system.[53] The molecular dynamics time step was 1 fs for a total of 1 ns, and the temperature coupling was iterated at 0.1 ps. The self-diffusion coefficient was calculated from the mean-square displacement of the particles using the Einstein relation

$$D = \lim_{t\to\infty} (\mathbf{r}(t) - \mathbf{r}(0))^2/6t$$

where $\mathbf{r}(t)$ denotes the position vector of a molecule at time t.

3. RESULTS AND DISCUSSION

Figure 2 shows the single-component adsorption of H_2O in (a) PAF-302, (c) PAF-303, and (e) PAF-304 and of CH_3OH in (b) PAF-302, (d) PAF-303, and (f) PAF-304 at 303 K. All materials adsorb much more CH_3OH than H_2O. More importantly, CH_3OH uptake increases with fullerene loading while H_2O uptake decreases with fullerene loading. Therefore, the incorporation of fullerenes will increase the selective ability of the framework. The highest H_2O adsorption is 0.46 mmol/g within PAF-304 with no fullerenes because of the large amount of pore volume. In contrast, the highest CH_3OH adsorption is 2 mmol/g within PAF-304 along with 104 fullerenes where organophilicity is maximized by a large amount of hydrophobic surface area. The key to maximizing separation efficiency is to increase both selectivity and uptake, as will be explored further the paper.

Figure 3 shows the equimolar adsorption of CH_3OH/H_2O from the simulated mixture (50:50). Once again, CH_3OH adsorption is much higher than that of H_2O. The hydrophobic structure of PAFs interacts more strongly with CH_3OH. Figures 3a−c show that the CH_3OH loading increases with fullerene loading. For 1 C_{60}@PAF-302 the highest CH_3OH adsorption is approximately 0.75 mmol/g. However, when incorporating the PAF-302 with 17C_{60}'s, an optimum condition, the uptake increased to ∼0.9 mmol/g. A similar pattern of CH_3OH adsorption is also observed for PAF-303 and PAF-304, when impregnated with C_{60}. The adsorption of CH_3OH in PAF-303 and PAF-304 are 1.56 and 1.65 mmol/g, respectively, when incorporated with the optimum number of fullerenes, namely 46C_{60}@PAF-303 and 104C_{60}@PAF-304, respectively. In these cases, the optimum amount of fullerenes is the maximum loading, meaning that there is enough porosity to adsorb significantly large amounts of methanol.

The mixture adsorption effect has more of a detrimental effect for H_2O adsorption than for CH_3OH. CH_3OH loading is approximately 1.94 mmol/g in 104 C_{60}@PAF-304 compared to the 1.65 mmol/g in mixture. On the other hand, there was a huge variation in H_2O adsorption for mixture with a ∼50% decrease compared to the single-component adsorption for all PAFs. Once again, the general trend of CH_3OH adsorption is increasing with fullerene impregnation for all PAFs, while for H_2O adsorption the trend is in reversed order; i.e., fullerene impregnation inhibits adsorption. The negligible adsorption of H_2O in mixture is due to the relatively large amount CH_3OH adsorption which blocks the available adsorption sites for H_2O.

The adsorption separation factor $S_{i/j} = (x_i/x_j)(y_j/y_i)$, where x_i and y_i are the mole fractions of component i in adsorbed phase and the bulk feed, respectively. In this study, the feed molar fractions are identical and therefore the separation factor is equal to the selectivity (= x_i/x_j). When comparing with other studies, the separation factors are converted to selectivities using this relation. As shown in Figure 4a, the highest selectivity of CH_3OH over H_2O is almost 1540, at 1 kPa for 17 C_{60}@PAF-302. For 46 C_{60}@PAF-303 and 104 C_{60}@PAF-304 the highest selectivities are 1481 and 1432 at 1 kPa (Figures 4b and 4c, respectively). The selectivity decreased gradually with increasing pressure. The reason behind this is the entropic effect.[54] The molecular size of H_2O is smaller than CH_3OH which allows a more efficient packing into the structures at high pressures. Meanwhile, a negligible selectivity is observed for all three bare PAFs with a highest value of 3.18 for PAF-302 at 1 kPa. This is comparable to

dx.doi.org/10.1021/la503547n | Langmuir 2014, 30, 14621−14630

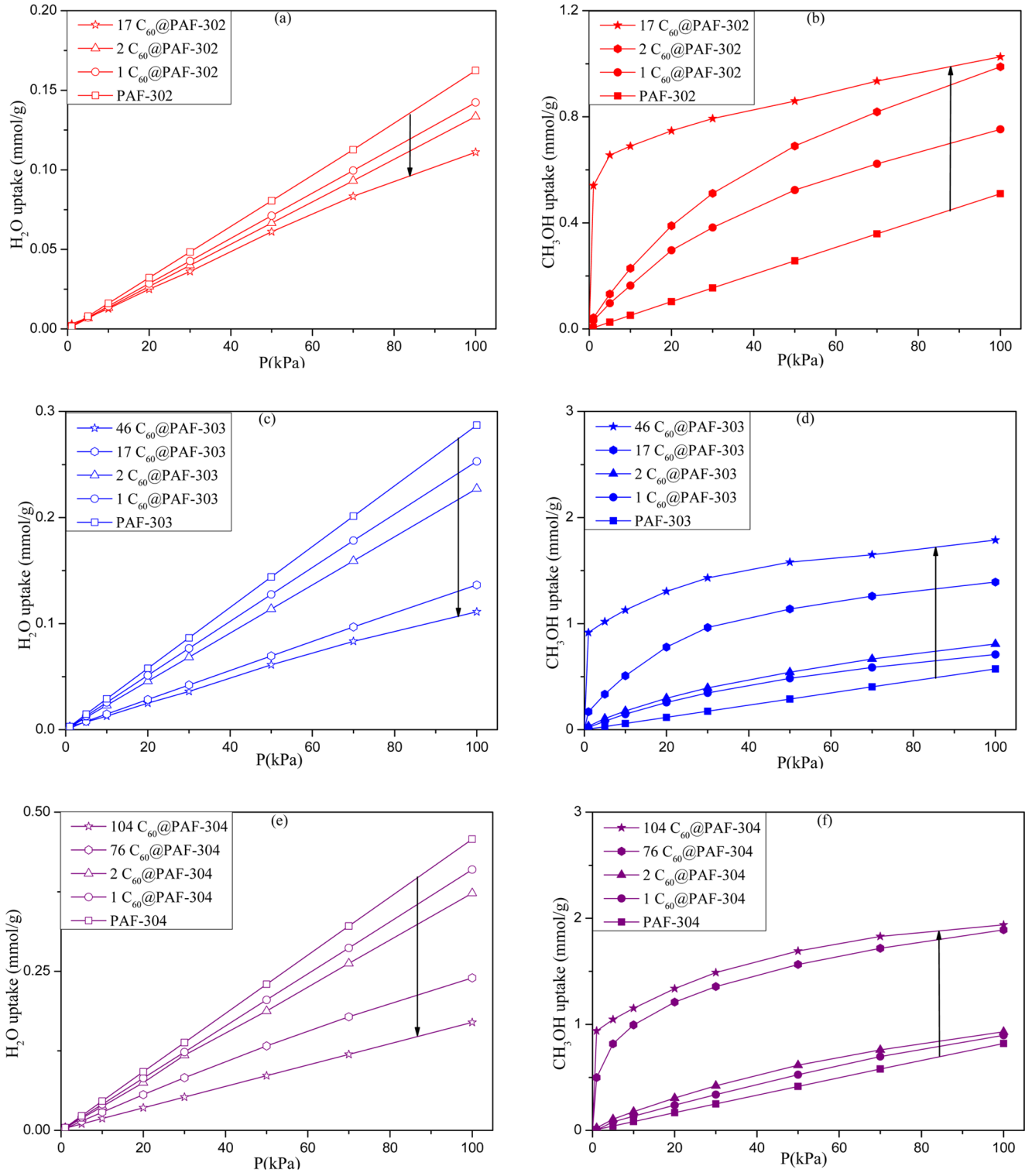

Figure 2. Total adsorption of single component (a) H_2O in PAF-302, (b) CH_3OH in PAF-302, (c) H_2O in PAF-303, (d) CH_3OH in PAF-303, (e) H_2O in PAF-304, and (f) CH_3OH in PAF-304 at 303 K.

the theoretical nonselective Knudsen selectivity value of 0.75. The selectivities showed a more enduring rise upward with the impregnation of C_{60} at low pressure. As a result, we can achieve a remarkable enhancement of selectivity in PAF-303 for an optimal number of fullerenes (C_{60}).

Figure 5 illustrates the selectivity vs CH_3OH uptake, which is a good indicator of performance efficiency. The higher the selectivity, the fewer separation stages are required, and the higher the CH_3OH uptake, the less material is required. Therefore, an ideal material sits in the high top right corner of this graph. It can be seen from Figure 3 that for all the three PAFs CH_3OH uptake increases with pressure but at a loss of selectivity. This phenomenon is also observed in the Robeson trade-off for polymer membranes,[55] where there are decreasing trends of gas selectivity with gas permeation. Fullerene impregnation, however, completely breaks this trend and is capable of

dx.doi.org/10.1021/la503547n | *Langmuir* 2014, 30, 14621−14630

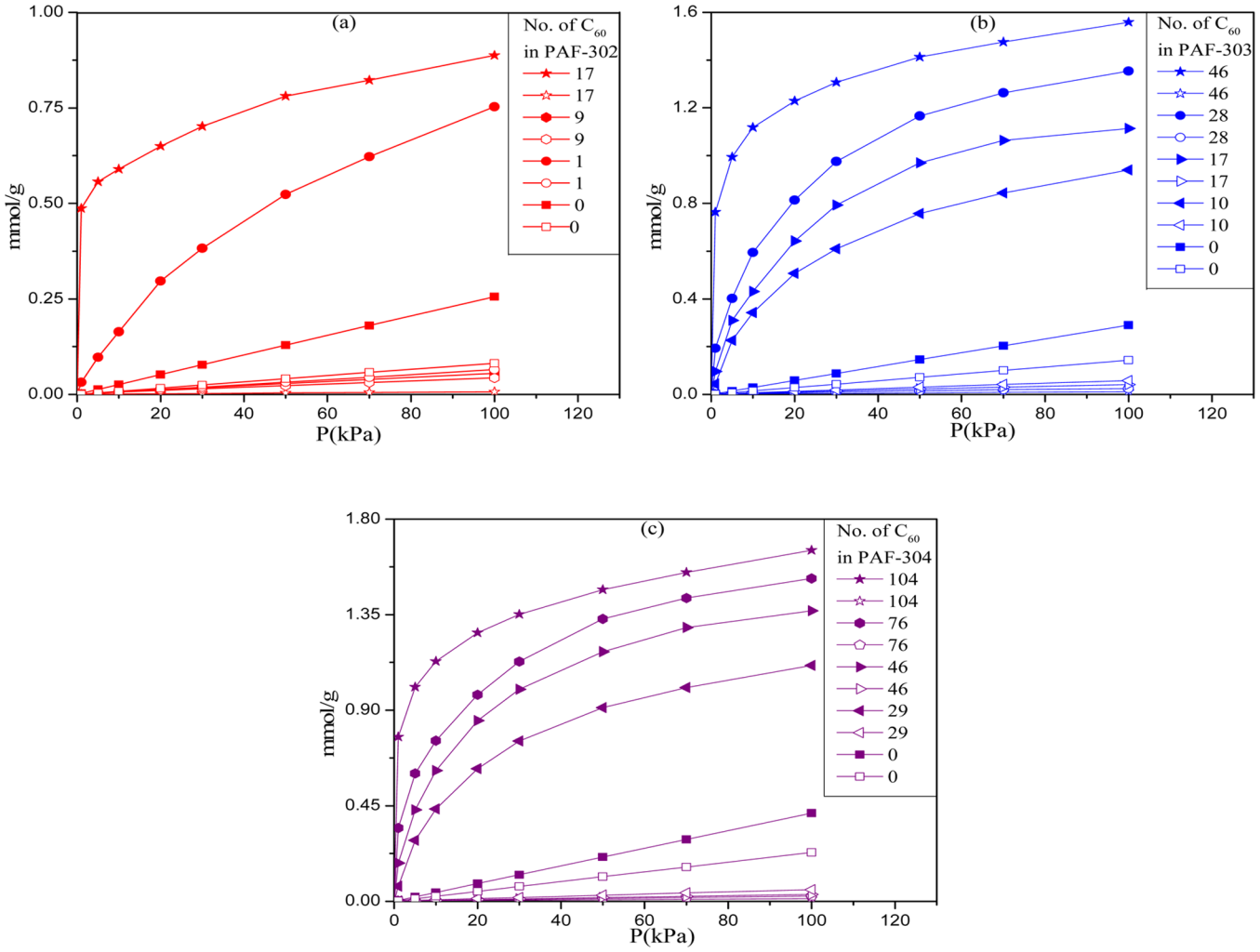

Figure 3. Adsorption of an equimolar mixture of CH_3OH/H_2O at 303 K in (a) PAF-302, (b) PAF-303, and (c) PAF-304. Closed symbols are for CH_3OH, and open symbols are for H_2O.

increasing selectivity simultaneously with uptake. These results show that fullerene impregnation of PAFs is a strategy for enhancing the separation efficiency of an adsorbent-based system. We have also compared our simulated results with some of the highest CH_3OH/H_2O selectivities of 1932 for ZSM-5 zeolite membrane,[6] 1000 for P84 copolyimide membrane,[56] and 20 for MOF adsorbent,[33] from the literature which are represented by the dashed lines in Figure 5. These results show that our adsorption-selective PAFs are among the highest performing separation materials.

We take a closer look at the adsorption behavior within the fullerene−PAF composites during simulation with molecular snapshots of the CH_3OH/H_2O mixture density in Figure 6. The highest performing materials are examined here, namely, (a) 17 C_{60}@ PAF-302, (b) 46 C_{60}@ PAF-303, and (c) 104 C_{60}@ PAF-304. In every case there is a substantially higher uptake of CH_3OH over H_2O, represented by the red and green dots, respectively. For further clarification we also calculated the density of CH_3OH and H_2O within the pore volume. For bare PAF-304 at 100 kPa the density of CH_3OH within the pores is twice as dense than the bulk phase (0.0854 mmol/cm^3 within PAF-304, 0.04 mmol/cm^3 bulk CH_3OH density) while the density of H_2O within the pores is similar as the bulk phase (0.047 mmol/cm^3 within PAF-304, 0.033 mmol/cm^3 bulk H_2O density). These values also indicate that there are weak interactions between the H_2O and bare PAF. For 104C_{60}@ PAF-304 these values are 6.8 and 0.6 mmol/cm^3, respectively. Thus, the hydrophobicity of the PAF framework and the fullerene surfaces combined ensures an unfavorable environment for the adsorption of water.

At this point, the impregnated PAFs are excellent candidates for adsorbent-based separations of methanol and water mixtures with enhanced selectivity and uptake. To assess the feasibility of these materials for membrane-based separations, we must examine their diffusion properties in addition to their adsorption properties.[57] In fact, a good estimate of transport flux (permeation) is the product of adsorbent loading and diffusivity, which is defined as the amount of molecules that pass through the material per time at a given pressure gradient. This means that if adsorption doubles and diffusivity halves, then the transport flux will remain constant. Therefore, we aim to maximize the transport flux of methanol over water, by either increasing the adsorption selectivity, diffusion selectivity, or both. Above we have observed an enormous increase in adsorption selectivity with fullerene impregnation.

Transport properties of liquids within confined pores depend on the molecule size, the pore size, and the molecular interactions with the pore surface. Transport of mixtures is even more complicated because of blocking effects and the mixed interactions between components. The average number of

dx.doi.org/10.1021/la503547n | *Langmuir* 2014, 30, 14621−14630

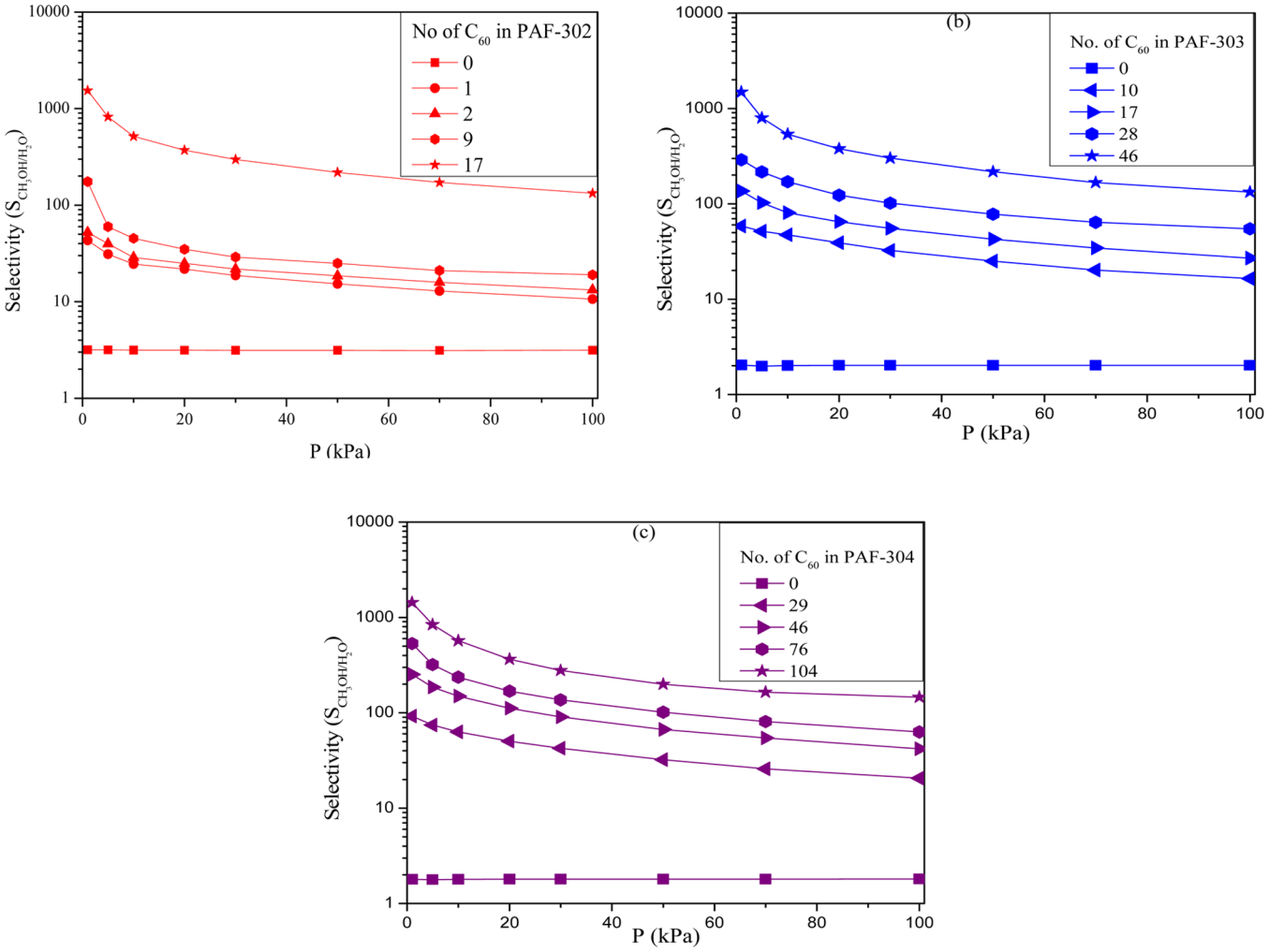

Figure 4. Selectivity of an equimolar mixture of CH_3OH/H_2O at 303 K in (a) PAF-302, (b) PAF-303, and (c) PAF-304.

hydrogen bonds per molecule for water and liquid methanol is 3.50 and 2, respectively, in bulk phase.[58,59] Within pores, these hydrogen bonds are disrupted due to the competing interactions with the pore surface. Hydrophobic pores such as nanotubes accelerate the diffusion of water because of the disrupted water orientation and weak water−pore interactions. On the other hand, ultrasmall pores may confine water and inhibit the diffusion. The impregnation of PAFs with C_{60} increases the hydrophobicity but also reduces the pore size.

The water and methanol self-diffusivities are calculated at bulk densities inside the bare PAF structures according to the methodology outlined earlier. Water and methanol bulk diffusivities were calculated as 5.21×10^{-9} and 1.97×10^{-9} m^2/s, respectively, which are consistent with the literature.[58,60,61] PAF-301 was incapable of hosting CH_3OH at the required densities and therefore has been omitted. In Figure 7, simulation results show that the self-diffusion coefficients of both H_2O and CH_3OH molecules increase with the increasing number of phenyl rings in the PAF structures. As expected, H_2O diffusion is greater in the PAF structures compared with the bulk diffusivity because of the hydrophobicity effect within the channels as discussed earlier. Jei et al.[57] have also reported that the transport of fluids inside the hydrophobic nanotubes is faster than fluids inside hydrophilic nanotubes. The enhancement in diffusion is much more dominant for H_2O than CH_3OH, which agrees with the principle of fast transport inside hydrophobic structures of increasing pore size. To explore the interactions and positions of CH_3OH and H_2O within the PAF structures, the radial distribution function $g(r)$ between the PAF-302 framework and the guest molecules is shown in Figure S4 of the Supporting Information. A high peak in $g(r)$ for CH_3OH is observed at $r = 5$ Å, indicating a high density of CH_3OH close to the PAF surface, whereas no significant peaks exist for H_2O indicating bulklike behavior. This confirms that CH_3OH interacts strongly with the PAF surface, forming a single adsorbed layer, while H_2O molecules interact weakly with the framework.

The equimolar mixture diffusivity results of CH_3OH and H_2O demonstrates more complex behavior. Here we simulate the mixture diffusivity within the optimized C_{60}@PAF structures which exhibited high adsorption performance, namely 17C_{60}@PAF-302, 46 C_{60}@PAF-303, and 104 C_{60}@PAF-304 in Figure 8. There is a decrease in both CH_3OH and H_2O diffusivity in the mixture system below the self-diffusivity simulated in the bulk phase and bare PAFs. The CH_3OH/H_2O diffusion selectivity of the mixture is 0.06, 0.16, and 1.88 for 17 C_{60}@PAF-302, 46 C_{60}@PAF-303, and 104 C_{60}@PAF-304, respectively. Therefore, the materials are more adsorption selective than diffusion selective. With the combined effects of mixed adsorption and diffusion, a maximum flux selectivity of 2692 could be achieved which is above any reported membrane selectivity, although higher pressures would be required for a membrane-based operation. In summary, our calculations predict that C_{60}@PAF-based

dx.doi.org/10.1021/la503547n | *Langmuir* 2014, 30, 14621−14630

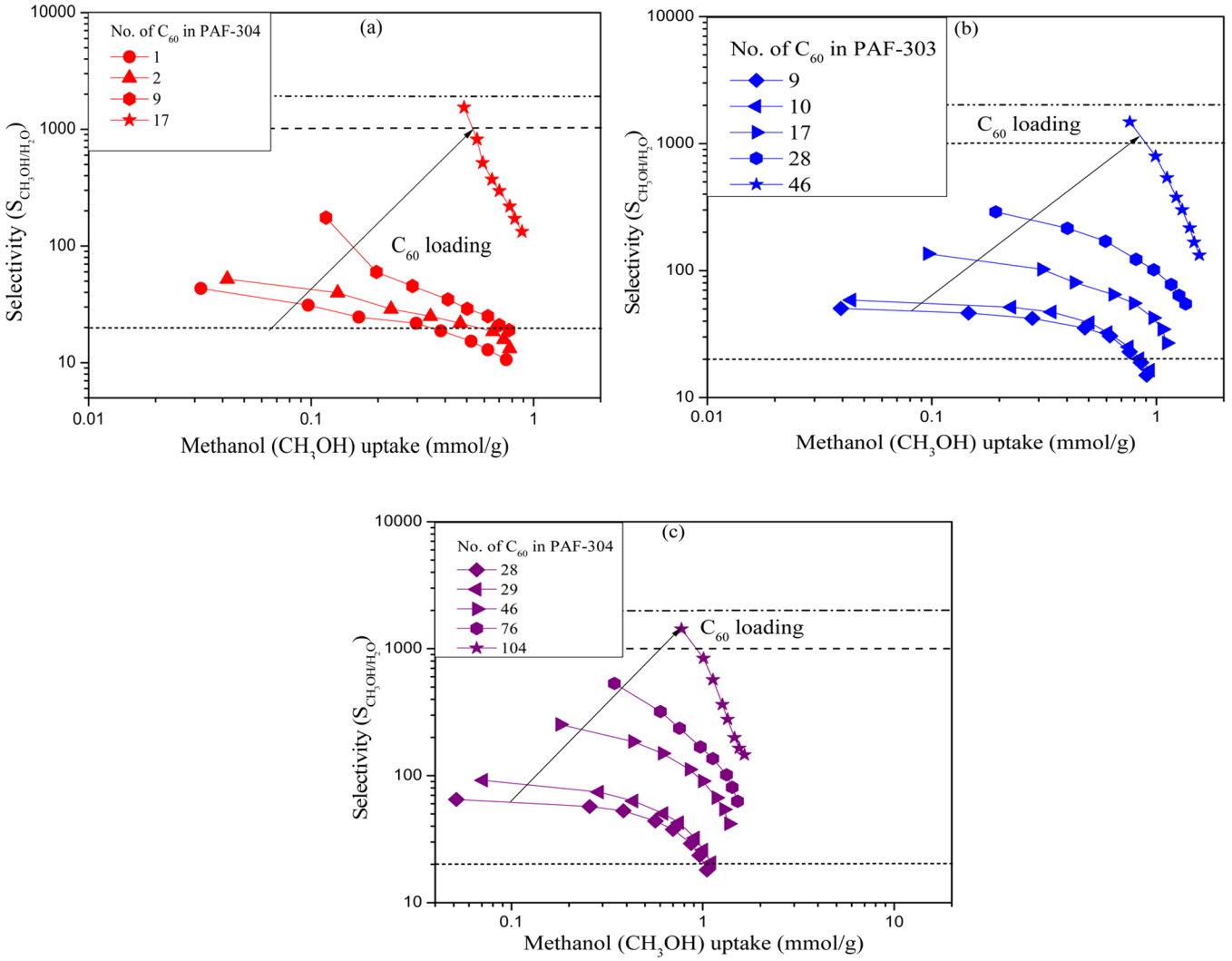

Figure 5. Selectivity vs CH_3OH uptake at 303 K in (a) PAF-302, (b) PAF-303, and (c) PAF-304, where dashed lines represent the selectivities (1932, 1000, and 20) of the highest performing materials in the literature.[6,33,56]

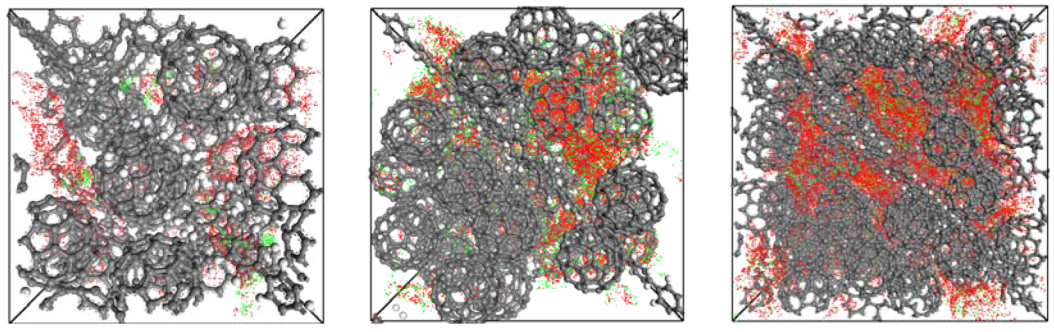

Figure 6. Snapshot of CH_3OH/H_2O adsorption uptake at 303 K and 100 kPa in (a) 17 C_{60}@ PAF-302, (b) 46 C_{60}@ PAF-303, and (c) 104 C_{60}@ PAF-304, where green and red dots are represent H_2O and CH_3OH density, respectively.

adsorbents and membranes would be strongly selective for CH_3OH over H_2O as a result of the significant adsorption and diffusion selectivity.

4. CONCLUSIONS

We have investigated the adsorption and diffusion of the CH_3OH/H_2O mixture by molecular simulation in extensively hydrophobic C_{60}@PAF structures. Despite the lack of experimental results, the simulated isotherms for pure components of CH_3OH and H_2O are in good agreement with experimental results of MOF and ZIFs from the literature.[33,62] The predicted adsorption selectivity of CH_3OH over H_2O is 1540 for 17C_{60}@PAF-302 with an additional diffusivity selectivity of around 3000 due to the dominant CH_3OH

dx.doi.org/10.1021/la503547n | *Langmuir* 2014, 30, 14621−14630

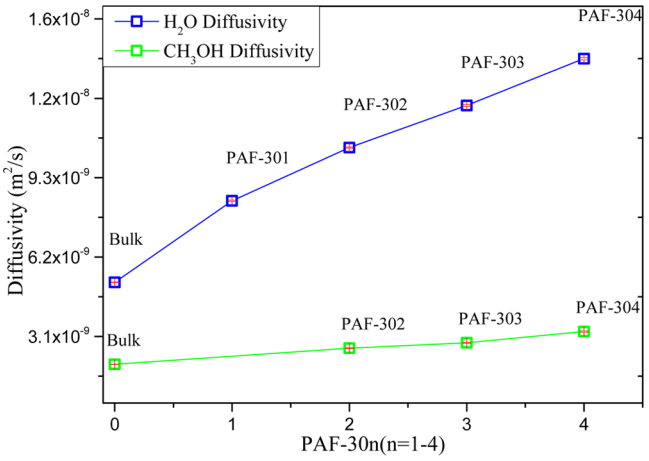

Figure 7. Self-diffusivity of H_2O and CH_3OH at 303 K in the available PAFs. Red indicates the error in calculations.

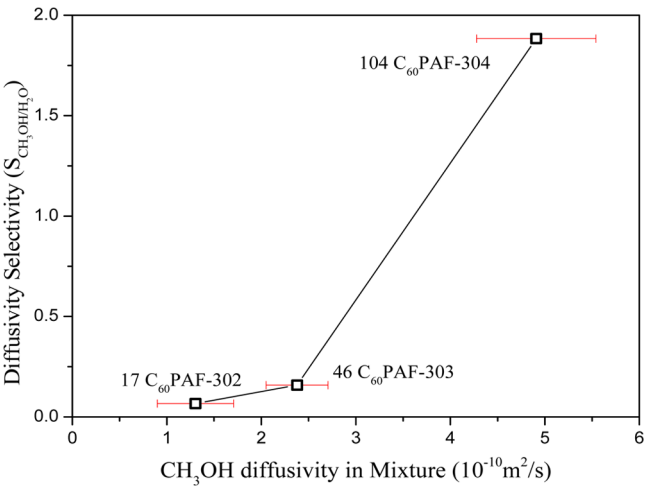

Figure 8. Diffusivity selectivity versus CH_3OH diffusivity in the mixture of CH_3OH/H_2O at 303 K. Red indicates the error in calculations.

adsorption. The hydrophobic properties of impregnated PAFs explain the negligible affinity for H_2O adsorption. The results show that the smaller pore volume of PAF-302 has a stronger interaction with CH_3OH compared to the other PAFs when impregnated with C_{60}'s. The high CH_3OH adsorption selectivity at low pressure suggests that C_{60}@PAF could be successfully used for the purification of CH_3OH from H_2O within an adsorbent-based separation system. Our simulations also predict that C_{60}@PAF may have promising properties for membrane-based separations that differentiate them in important ways from other membrane separation technologies. As a result, we can use less material for larger selectivities (~2500) and higher production rates (~1 mmol/g), which makes them cost-effective compared to other materials.

■ ASSOCIATED CONTENT

Supporting Information

Figures S1–S4 and Table S1. This material is available free of charge via the Internet at http://pubs.acs.org.

■ AUTHOR INFORMATION

Corresponding Author

*Tel +61418438423; e-mail aaron.thornton@csiro.au (A.W.T.).

Notes

The authors declare no competing financial interest.

■ ACKNOWLEDGMENTS

A.A. acknowledges the top-up scholarship provided by the CSIRO Computational and Simulation Sciences Transformational Capability Platform and the full scholarship provided by Swinburne University. The authors acknowledge the computational facilities and services provided through the CSIRO Advanced Scientific Computing.

■ REFERENCES

(1) Aasberg-Petersen, K.; Nielsen, C. S.; Dybkjær, I.; Perregaard, J. *Large Scale Methanol Production from Natural Gas*; Haldor Topsoe: Lyngby, Denmark, 2008; pp 1–14.

(2) Liu, Q.; Noble, R.; Falconer, J. L.; Funke, H. Organics/water separation by pervaporation with a zeolite membrane. *J. Membr. Sci.* **1996**, *117* (1), 163–174.

(3) Wijmans, J.; Baker, R.; Athayde, A. Pervaporation: removal of organics from water and organic/organic separations. In *Membrane Processes in Separation and Purification*; Springer: Berlin, 1994; pp 283–316.

(4) Fleming, H. L.; Slater, C. S. Applications and economics. In *Membrane Handbook*; Springer: Berlin, 1992; pp 132–159.

(5) Martin, N. *Removal of Methanol by Pervaporation*, Sulzer Chemtech, 19.01.2003.

(6) Tuan, V. A.; Li, S.; Falconer, J. L.; Noble, R. D. Separating organics from water by pervaporation with isomorphously-substituted MFI zeolite membranes. *J. Membr. Sci.* **2002**, *196* (1), 111–123.

(7) Han, S. S.; Furukawa, H.; Yaghi, O. M.; Goddard, W. A. Covalent organic frameworks as exceptional hydrogen storage materials. *J. Am. Chem. Soc.* **2008**, *130* (35), 11580–11581.

(8) Lan, J.; Cao, D.; Wang, W.; Ben, T.; Zhu, G. High-capacity hydrogen storage in porous aromatic frameworks with diamond-like structure. *J. Phys. Chem. Lett.* **2010**, *1* (6), 978–981.

(9) Zhong, Z.; Xiong, Z.; Sun, L.; Luo, J.; Chen, P.; Wu, X.; Lin, J.; Tan, K. Nanosized nickel (or cobalt)/graphite composites for hydrogen storage. *J. Phys. Chem. B* **2002**, *106* (37), 9507–9513.

(10) Cao, D.; Lan, J.; Wang, W.; Smit, B. Lithium-doped 3D covalent organic frameworks: high-capacity hydrogen storage materials. *Angew. Chem., Int. Ed.* **2009**, *48* (26), 4730–3.

(11) Kaye, S. S.; Dailly, A.; Yaghi, O. M.; Long, J. R. Impact of preparation and handling on the hydrogen storage properties of Zn_4O(1,4-benzenedicarboxylate)$_3$ (MOF-5). *J. Am. Chem. Soc.* **2007**, *129* (46), 14176–14177.

(12) Frost, H.; Düren, T.; Snurr, R. Q. Effects of surface area, free volume, and heat of adsorption on hydrogen uptake in metal–organic frameworks. *J. Phys. Chem. B* **2006**, *110* (19), 9565–9570.

(13) Ben, T.; Pei, C.; Zhang, D.; Xu, J.; Deng, F.; Jing, X.; Qiu, S. Gas storage in porous aromatic frameworks (PAFs). *Energy Environ. Sci.* **2011**, *4* (10), 3991–3999.

(14) Ben, T.; Ren, H.; Ma, S.; Cao, D.; Lan, J.; Jing, X. Targeted synthesis of a porous aromatic framework with high stability and exceptionally high surface area. *Angew. Chem.* **2009**, *48* (50), 9457–9460.

(15) Ren, H.; Ben, T.; Wang, E.; Jing, X.; Xue, M.; Liu, B.; Cui, Y.; Qiu, S.; Zhu, G. Targeted synthesis of a 3D porous aromatic framework for selective sorption of benzene. *Chem. Commun.* **2010**, *46* (2), 291–293.

(16) Ren, H.; Ben, T.; Sun, F.; Guo, M.; Jing, X.; Ma, H.; Cai, K.; Qiu, S.; Zhu, G. Synthesis of a porous aromatic framework for adsorbing organic pollutants application. *J. Mater. Chem.* **2011**, *21* (28), 10348–10353.

(17) Babarao, R.; Dai, S.; Jiang, D.-E. Functionalizing porous aromatic frameworks with polar organic groups for high-capacity and selective CO_2 separation: A molecular simulation study. *Langmuir* **2011**, *27* (7), 3451–3460.

(18) Yuan, Y.; Sun, F.; Ren, H.; Jing, X.; Wang, W.; Ma, H.; Zhao, H.; Zhu, G. Targeted synthesis of a porous aromatic framework with a high

adsorption capacity for organic molecules. *J. Mater. Chem.* **2011**, *21* (35), 13498−13502.
(19) Ben, T.; Li, Y.; Zhu, L.; Zhang, D.; Cao, D.; Xiang, Z.; Yao, X.; Qiu, S. Selective adsorption of carbon dioxide by carbonized porous aromatic framework (PAF). *Energy Environ. Sci.* **2012**, *5* (8), 8370−8376.
(20) Li, Y.; Ben, T.; Zhang, B.; Fu, Y.; Qiu, S. Ultrahigh gas storage both at low and high pressures in KOH-activated carbonized porous aromatic frameworks. *Sci. Rep.* **2013**, *3*.
(21) Ma, H.; Ren, H.; Zou, X.; Meng, S.; Sun, F.; Zhu, G. Post-metalation of porous aromatic frameworks for highly efficient carbon capture from CO_2 + N_2 and CH_4 + N_2 mixtures. *Polym. Chem.* **2014**, *5*, 144−152.
(22) Yan, Z.; Ren, H.; Ma, H.; Yuan, R.; Yuan, Y.; Zou, X.; Sun, F.; Zhu, G. Construction and sorption properties of pyrene-based porous aromatic frameworks. *Microporous Mesoporous Mater.* **2013**.
(23) Pei, C.; Ben, T.; Cui, Y.; Qiu, S. Storage of hydrogen, methane, carbon dioxide in electron-rich porous aromatic framework (JUC-Z2). *Adsorption* **2012**, *18* (5−6), 375−380.
(24) Garibay, S. J.; Weston, M. H.; Mondloch, J. E.; Colón, Y. J.; Farha, O. K.; Hupp, J. T.; Nguyen, S. T. Accessing functionalized porous aromatic frameworks (PAFs) through a de novo approach. *CrystEngComm* **2013**, *15* (8), 1515−1519.
(25) Konstas, K.; Taylor, J. W.; Thornton, A. W.; Doherty, C. M.; Lim, W. X.; Bastow, T. J.; Kennedy, D. F.; Wood, C. D.; Cox, B. J.; Hill, J. M. Lithiated porous aromatic frameworks with exceptional gas storage capacity. *Angew. Chem., Int. Ed.* **2012**, *124* (27), 6743−6746.
(26) Lau, C. H.; Nguyen, P. T.; Hill, M. R.; Thornton, A. W.; Konstas, K.; Doherty, C. M.; Mulder, R. J.; Bourgeois, L.; Liu, A. C.; Sprouster, D. J. Ending aging in super glassy polymer membranes. *Angew. Chem., Int. Ed.* **2014**, *53*, 5322−5326.
(27) Zheng, J.; Lennon, E. M.; Tsao, H.-K.; Sheng, Y.-J.; Jiang, S. Transport of a liquid water and methanol mixture through carbon nanotubes under a chemical potential gradient. *J. Chem. Phys.* **2005**, *122*, 214702.
(28) Palinkas, G.; Hawlicka, E.; Heinzinger, K. A molecular dynamics study of liquid methanol with a flexible three-site model. *J. Phys. Chem.* **1987**, *91* (16), 4334−4341.
(29) Nalaparaju, A.; Zhao, X.; Jiang, J. Molecular understanding for the adsorption of water and alcohols in hydrophilic and hydrophobic zeolitic metal− organic frameworks. *J. Phys. Chem. C* **2010**, *114* (26), 11542−11550.
(30) Chen, B.; Ji, Y.; Xue, M.; Fronczek, F. R.; Hurtado, E. J.; Mondal, J. U.; Liang, C.; Dai, S. Metal− organic framework with rationally tuned micropores for selective adsorption of water over methanol. *Inorg. Chem.* **2008**, *47* (13), 5543−5545.
(31) James, S. L. Metal-organic frameworks. *Chem. Soc. Rev.* **2003**, *32* (5), 276−288.
(32) de Lima, G. F.; Mavrandonakis, A.; de Abreu, H. A.; Duarte, H. A.; Heine, T. Mechanism of alcohol−water separation in metal−organic frameworks. *J. Phys. Chem. C* **2013**, *117* (8), 4124−4130.
(33) Chen, Y. F.; Lee, J. Y.; Babarao, R.; Li, J.; Jiang, J. W. A Highly hydrophobic metal−organic framework $Zn(BDC)(TED)_{0.5}$ for adsorption and separation of CH_3OH/H_2O and CO_2/CH_4: An integrated experimental and simulation study. *J. Phys. Chem. C* **2010**, *114* (14), 6602−6609.
(34) Ahmed, A.; Thornton, A. W.; Konstas, K.; Kannam, S. K.; Babarao, R.; Todd, B. D.; Hill, A. J.; Hill, M. R. Strategies toward enhanced low-pressure volumetric hydrogen storage in nanoporous cryoadsorbents. *Langmuir* **2013**, *29* (50), 15689−15697.
(35) Hill, A. J.; Jones, P. L.; Lind, J. H.; Pearsall, G. W. A positron annihilation lifetime study of isothermal structural relaxation in bisphenol-A polycarbonate. *J. Polym. Sci., Part A: Polym. Chem.* **1988**, *26*, 1541−1552.
(36) Wang, X. Y.; Lee, K. M.; Lu, Y.; Stone, M. T.; Sanchez, I. C.; Freeman, B. D. Cavity size distributions in high free volume glassy polymers by molecular simulation. *Polymer* **2004**, *45* (11), 3907−3912.
(37) Mayo, S. L.; Olafson, B. D.; Goddard, W. A. DREIDING: a generic force field for molecular simulations. *J. Phys. Chem.* **1990**, *94* (26), 8897−8909.
(38) Wallqvist, A. Molecular dynamics study of hydrophobic aggregation in water/methane/methanol systems. *Chem. Phys. Lett.* **1991**, *182* (3−4), 237−241.
(39) Haughney, M.; Ferrario, M.; McDonald, I. R. Molecular-dynamics simulation of liquid methanol. *J. Phys. Chem.* **1987**, *91* (19), 4934−4940.
(40) Nguyen, V. T.; Do, D.; Nicholson, D.; Jagiello, J. Effects of temperature on adsorption of methanol on graphitized thermal carbon black: a computer simulation and experimental study. *J. Phys. Chem. C* **2011**, *115* (32), 16142−16149.
(41) Birkett, G.; Do, D. Simulation study of methanol and ethanol adsorption on graphitized carbon black. *Mol. Simul.* **2006**, *32* (10−11), 887−899.
(42) Jorgensen, W. L. Optimized intermolecular potential functions for liquid alcohols. *J. Phys. Chem.* **1986**, *90* (7), 1276−1284.
(43) Yang, Z.; Peng, X.; Cao, D. Carbon dioxide capture by PAFs and an efficient strategy to fast screen porous materials for gas separation. *J. Phys. Chem. C* **2013**, *117* (16), 8353−8364.
(44) Sun, Y.; Kollman, P. A. Hydrophobic solvation of methane and nonbond parameters of the TIP3P water model. *J. Comput. Chem.* **1995**, *16* (9), 1164−1169.
(45) Young, W. S.; Brooks Iii, C. L. A reexamination of the hydrophobic effect: Exploring the role of the solvent model in computing the methane−methane potential of mean force. *J. Chem. Phys.* **1997**, *106* (22), 9265−9269.
(46) Mark, P.; Nilsson, L. Structure and dynamics of the TIP3P, SPC, and SPC/E water models at 298 K. *J. Phys. Chem. A* **2001**, *105* (43), 9954−9960.
(47) Kwak, T.; Mansoori, G. Van der Waals mixing rules for cubic equations of state. Applications for supercritical fluid extraction modelling. *Chem. Eng. Sci.* **1986**, *41* (5), 1303−1309.
(48) van Leeuwen, M. E.; Smit, B. Molecular simulation of the vapor-liquid coexistence curve of methanol. *J. Phys. Chem.* **1995**, *99* (7), 1831−1833.
(49) Haughney, M.; Ferrario, M.; McDonald, I. R. Pair interactions and hydrogen-bond networks in models of liquid methanol. *Mol. Phys.* **1986**, *58* (4), 849−853.
(50) Shevade, A. V.; Jiang, S.; Gubbins, K. E. Adsorption of water—methanol mixtures in carbon and aluminosilicate pores: a molecular simulation study. *Mol. Phys.* **1999**, *97* (10), 1139−1148.
(51) Zhang, Q.; Zheng, J.; Shevade, A.; Zhang, L.; Gehrke, S. H.; Heffelfinger, G. S.; Jiang, S. Transport diffusion of liquid water and methanol through membranes. *J. Chem. Phys.* **2002**, *117*, 808.
(52) Thornton, A. W.; Nairn, K. M.; Hill, J. M.; Hill, A. J.; Hill, M. R. Metal-organic frameworks impregnated with magnesium-decorated fullerenes for methane and hydrogen Storage. *J. Am. Chem. Soc.* **2009**, *131* (30), 10662−10669.
(53) Mahoney, M. W.; Jorgensen, W. L. Diffusion constant of the TIP5P model of liquid water. *J. Chem. Phys.* **2001**, *114* (1), 363−366.
(54) Krishna, R. Diffusion of binary mixtures across zeolite membranes: entropy effects on permeation selectivity. *Int. Commun. Heat Mass Transfer* **2001**, *28* (3), 337−346.
(55) Robeson, L. M. The upper bound revisited. *J. Membr. Sci.* **2008**, *320* (1−2), 390−400.
(56) Qiao, X.; Chung, T.-S.; Pramoda, K. Fabrication and characterization of BTDA-TDI/MDI (P84) co-polyimide membranes for the pervaporation dehydration of isopropanol. *J. Membr. Sci.* **2005**, *264* (1), 176−189.
(57) Zheng, J.; Lennon, E. M.; Tsao, H.-K.; Sheng, Y.-J.; Jiang, S. Transport of a liquid water and methanol mixture through carbon nanotubes under a chemical potential gradient. *J. Chem. Phys.* **2005**, *122*, 214702.
(58) Shevade, A. V.; Jiang, S.; Gubbins, K. E. Molecular simulation study of water-methanol mixtures in activated carbon pores. *J. Chem. Phys.* **2000**, *113* (16), 6933−6942.
(59) Jorgensen, W. L.; Chandrasekhar, J.; Madura, J. D.; Impey, R. W.; Klein, M. L. Comparison of simple potential functions for simulating liquid water. *J. Chem. Phys.* **1983**, *79* (2), 926−935.
(60) Raabe, G.; Sadus, R. J. Molecular simulation of the vapor−liquid coexistence of mercury. *J. Chem. Phys.* **2003**, *119*, 6691.

(61) Mahoney, M. W.; Jorgensen, W. L. A five-site model for liquid water and the reproduction of the density anomaly by rigid, nonpolarizable potential functions. *J. Chem. Phys.* **2000**, *112*, 8910.
(62) Kuhn, J.; Castillo-Sanchez, J. M.; Gascon, J.; Calero, S.; Dubbeldam, D.; Vlugt, T. J. H.; Kapteijn, F.; Gross, J. Adsorption and diffusion of water, methanol, and ethanol in all-silica DD3R: Experiments and simulation. *J. Phys. Chem. C* **2009**, *113* (32), 14290−14301.